Desalination and Water Treatment
www.deswater.com

doi:10.5004/dwt.2019.23488

141 (2019) 51–67
February

Effect of Ca^{2+} on organic fouling of hydrophobic polytetrafluoroethylene membrane during membrane distillation process: an especial interest in intermolecular interactions

Chang Liu[a,b], Lin Chen[a,b,*], Liang Zhu[a,b,*]

[a]*Key Laboratory of Integrated Regulation and Resources Development of Shallow Lakes, Hohai University, Nanjing 210098, China, email: 15850600312@163.com (C. Liu), chen_lin@hhu.edu.cn (L. Chen), hhuzhuliang@163.com (L. Zhu)*
[b]*College of Environment, Hohai University, Nanjing 210098, China*

Received 8 May 2018; Accepted 18 November 2018

ABSTRACT

The growing attention to membrane distillation (MD) processes from various disciplines raises the demand for in-depth research on MD membrane fouling. This study investigates the role of salt ions, such as Ca^{2+}, in organic fouling of direct contact membrane distillation (DCMD). The differently charged lysozyme (LYS), sodium alginate (SA), and bovine serum albumin (BSA) were chosen as model organic foulants. The fouling data showed that Ca^{2+} obviously aggravated the flux decline rate from 0.55 ~ 0.67 to 0.35 ~ 0.61. The scanning electron microscopy coupled with energy dispersion spectrometry (SEM-EDX) analysis further displayed that Ca^{2+} could cause higher mass deposition on the membrane surface and correspondingly severe fouling behavior. Through the gel permeation chromatography (GPC) analysis, obvious binding interactions between foulants were observed as a result of the decisive role of Ca^{2+}, finally leading to the significant changes of zeta potential and particle size of feed solutions. The zeta potential obviously decreased with a trend towards the neutral state, and the particle size increased except for the individual LYS. Additionally, the interfacial interaction analysis was applied to study the foulant-membrane and foulant-foulant interaction energy, and the results showed that Ca^{2+} significantly decreased the repulsive electrostatic interaction energy between foulants and membrane surface, leading to a severe foulants deposition and membrane fouling.

Keywords: Membrane distillation; Organic fouling; Calcium ion; Intermolecular interaction; Interfacial interaction energy

1. Introduction

Membrane distillation (MD), a potential alternative to widely applied pressure-driven membrane processes such as microfiltration (MF), ultrafiltration (UF), nanofiltration (NF) and reverse osmosis (RO) in the fields of industrial wastewater treatment, domestic wastewater reclamation and seawater desalination, is gaining widespread attention in recent years [1]. This novel membrane-based water treatment technology is a thermally-driven separation process, using trans-membrane vapor pressure difference as driving force [2].

Similar to other membrane separation processes, membrane fouling is still an unresolved problem [3], which can lead to significant permeate flux decline as well as serious deterioration of effluent quality [4]. In order to figure out the membrane fouling mechanism, some researchers have been committed to the investigation of membrane fouling during the MD process. Tijing et al. [5] systematically reviewed the membrane fouling and its control strategies during the MD process. It was found that the salt crystallization and organic fouling were the main obstacles for the application of MD in wastewater treatment. Aiming

*Corresponding author.

at the membrane scaling, Nghiem and Cath [6] researched the scaling mechanism of direct contact membrane distillation (DCMD) process, and the results revealed that the membrane scaling was mainly caused by $CaSO_4$ in comparison with $CaCO_3$ and silicate. Except the inorganic fouling, Gryta et al. [7] also investigated the MD fouling during the treatment of NaCl solution containing natural organic matters. It was found that serious organic fouling was mainly caused by organic foulants including polysaccharide, proteins and humic-like substances. Additionally, the divalent ions, such as Ca^{2+} and Mg^{2+}, which are commonly found in seawater, wastewater, surface water and groundwater, can also affect the organic fouling process [8]. To our best knowledge, the influence of divalent ions on organic fouling for the DCMD process hasn't been researched until now. Although the effect of Ca^{2+} on organic fouling has already been partly researched in other membrane separation process, the heating condition, as a feature of the MD treatment process, can obviously affect the foulant properties and then the intermolecular interactions between foulants and Ca^{2+}, finally resulting in a significantly different fouling behavior for MD process. Furthermore, it has been widely reported that the process of foulant adhesion and cake layer formation was directly determined by the interfacial interactions, which was considered as the dominant factor of membrane fouling [9–11]. The interfacial interactions between organic foulants and membrane surface can be generally interpreted through the extended Derjaguin-Landau-Verwey-Overbeek (XDLVO) theory, which accounts for van der Waals (*LW*), electrostatic double layer (*EL*) and Lewis acid-base (*AB*) interactions [12,13]. The XDLVO model have been reported to be a viable method to qualitatively and quantitatively analyze those three types of interaction energies between foulants and membrane surface in MF, UF and RO processes [14–16]. And the XDLVO model can be expected to analyze the foulants adhesion on the MD membranes. Therefore, the XDLVO analysis was conducted to research the effect of Ca^{2+} on the interfacial interactions between organic foulants and MD membrane in this study, which may offer a new approach contributing to recognize and resolve membrane fouling in MD system.

Therefore, this study was aimed to investigate the role of Ca^{2+} on organic fouling of DCMD. The organic substances, including protein and polysaccharide, are the common foulants in wastewater [7,17,18]. Thus three kinds of organic macromolecules-serum albumin (BSA), lysozyme (LYS) and sodium alginate (SA) were chosen as model organics to prepare the synthetic feed solutions. The flux decline behavior was studied in detail with and without Ca^{2+}. Additionally, the effect of Ca^{2+} on membrane fouling degree was further analyzed by a scanning electron microscopy (SEM) coupled with energy dispersion spectrometry (EDX). To investigate the organic fouling mechanism of DCMD at the molecular level, the interfacial interaction energy between foulants and membrane surface was calculated through the XDLVO model. Moreover, to obtain further insight into the protein-polysaccharide complex formation and the pathways of organics aggregation, gel permeation chromatography (GPC) was applied to study the formation of protein-alginate complexes in the absence and presence of Ca^{2+}. In this way, the effect of Ca^{2+} on organic fouling mechanisms of DCMD can be deeply figured out, which will help to develop an effective mitigation approach for organic fouling control during DCMD operation.

2. Materials and methods

2.1. Bench-scale DCMD fouling experiment

The DCMD fouling experiment was conducted with a laboratory-scale DCMD system. A piece of polytetrafluoroethylene (PTFE) flat-sheet hydrophobic membrane (Taoyuan Medical and Chemical Factory, China) of 50.0 cm^2 effective areas was assembled inside the module, with the pore size of 0.22 μm, thickness of 190.0 μm and porosity of 75–80%. According to the preliminary experiment, the temperature for feed and permeate side was set as 75 and 15°C, respectively, which were controlled by a thermostat water bath and a cooler. Additionally, the peristaltic pumps were used to generate cross-flow velocity, with a suitable speed of 10.5 mm/s during the DCMD operation. The pure water permeability of virgin PTFE membrane was in a range of 13.27~14.36l/(m^2*h) under this experimental condition.

The membrane flux was derived by mass balance accounting for the membrane area, and then normalized for clean membrane flux to avoid the systematic error for each membrane. The normalized flux (NF) is calculated by the following equation:

$$NF = J/J_0 \tag{1}$$

where NF, J and J_0 are normalized flux, permeate flux and initial flux of each membrane, respectively. The tank for permeate collection was placed on a digital scale (BS-3000+) and the weight changes were monitored by a computer per 10 min to calculate the flux (J_0 or J). At the beginning of each fouling experiment, the initial flux (J_0) was measured by operating with the deionized water (DI) water for 6–8 h. And then the stock feed solution was added into the feed tank and continuously mixed by a magnetic stirrer. The fouling experiments were totally lasted for 4 d.

2.2. Model organic foulants and feed solution composition

BSA (69003433, Sinopharm), LYS (64006060, Sinopharm) and SA (30164428, Sinopharm) were chosen as model organic foulants with different charge properties. Under the testing condition (pH of 5–8, room temperature of 25°C), the BSA, LYS and SA represented negatively-charged protein, positively-charged protein and negatively-charged polysaccharide-like substances, respectively. According to the manufacturer, the molecular weights of BSA, LYS and SA were 66.0, 14.3 and 12.0–80.0 kDa, respectively. Each reagent was received in powder form with purity over 98%.

To accelerate the fouling rate, an extremely high concentration of 150 mg/L was applied in each experiment. The feed solutions were prepared 1 d in advance by dissolving the reagents into DI water, with an aim to ensure the complete dissolution. The total foulant concentration in feed solution was 150 mg/L, and only the mass ratio of BSA (or LYS) to SA (0%:100%, 50%:50%, or 100%:0%) was varied to study the effect of Ca^{2+} on membrane fouling behavior under different feed compositions. When investigating the

effect of Ca^{2+}, the calcium chloride ($CaCl_2$, PTS11245391, Sinopharm) stock solution with concentration of 10 mmol/L was added into the feed solution. Additionally, the pH of feed was initially adjusted to around 7 by the addition of HCl or NaOH.

2.3. Zeta potential and size measurement

The zeta potential and particle size of feed solution were measured by a laser particle analyzer (Nano-ZS90, Malvern Zetasizer), and each sample was measured for 3 times to avoid the accidental error. The effective monitoring range was 0.3~5 μm for this laser particle analyzer. If the particle size of mixed feed was above the detection limit (5 μm), another laser particle analyzer (Mastersizer 2000, Malvern Zetasizer) was then used for the size measurement of mixed feed solution.

Additionally, the zeta potential of membrane was measured by the tangential streaming potential method [19] using the electro kinetic analyzer (Sur PASS, Anton Paar).

2.4. Isoelectric point (IEP) of 75°C heated protein solution

According to the amphoteric dissociation properties, the solubility of protein would reach to the lowest value when the pH of solution was near to its *IEP* [20]. The *IEP* of BSA and LYS was measured according to the method that reported by Wintersteiner and A. Abramson [21].

2.5. Gel permeation chromatography (GPC)

Feed solution samples were analyzed by a SB-806M HQ size exclusion column (13 μm, 8.0 mm I.D. × 300 mm L) (Waters, America) equipped with a refractive index detector (RID, OPTILAB rEX, Wyatt, America). All sample injections were firstly filtered through an Acrodisc PES syringe filter (0.45 μm, Pall Corporation), and then an individual sample of 200 μL was injected for isocratic elution for 20 min with a flow rate of 0.5 ml/min. Additionally, the $NaNO_3$ solution with a concentration of 0.5 mol/L was used as mobile phase during the GPC measurement.

2.6. Membrane characterization

The morphology and elemental composition of the fouling layer were investigated by SEM (S-4800,HITACHI) coupled with EDX (OCTANE PLUS, AMETEK).

The attenuated total reflectance Fourier transform infrared spectroscopy (FTIR) (TENSOR 27, BRUKER) was used to identify the functional groups associated with MD membrane fouling.

2.7. Contact angle measurement

Contact angles were measured using DI water, formamide and diiodomethane to determine the surface tensions of PTFE membrane and different foulants [22]. The high-accuracy contact angle measurement was implemented by a new method-Drop Snake, which was based on B-spline snakes to shape the sessile drop [23]. Detailedly, the contact angle measurement of membrane was directly carried out on the membrane surface. Additionally, the contact angle analysis of foulant was conducted according to the method reported by Xiao et al. [22], and the specific pretreatment method for the organic foulant was that the foulant-water solutions were firstly 75°C heated in a water bath with an aim to keep consistent with the actual experimental conditions of the MD process.

2.8. Interaction energy measurement

According to the XDLVO theory, the total interaction energy (E_{ToT}) of particle-surface was mainly consisted of electrostatic interaction energy (E_{EL}), Lifshitz-van der Waals interaction energy (E_{LW}) and Lewis acid-base interaction energy (E_{AB}). Therefore, the interaction energy per unit area for *LW*, *AB* and *EL* is specifically calculated as the following equations:

$$E_{TOT} = E_{LW} + E_{AB} + E_{EL} \tag{2}$$

$$E_{LW}(h) = -\frac{A}{12\pi h^2} \tag{3}$$

$$E_{AB}(h) = \Delta G_{h_0}^{AB} \exp\left(\frac{h_0 - h}{\lambda}\right) \tag{4}$$

$$E_{EL}(h) = \varepsilon_r \varepsilon_0 \kappa \xi_1 \xi_3 \left[\frac{\xi_1^2 + \xi_3^2}{2\xi_1 \xi_3} (1\text{-}\coth \kappa h) + \frac{1}{\sinh \kappa h} \right] \tag{5}$$

where $A = -12\pi h_0^2 \Delta G_{h_0}^{LW}$ is the Hamaker constant; h_0 is the minimum cut-off distance due to Born repulsion (h_0 = 0.158 nm) [24]; $\Delta G_{h_0}^{LW} = 2(\sqrt{r_2^{LW}} - \sqrt{r_1^{LW}})(\sqrt{r_3^{LW}} - \sqrt{r_2^{LW}})$ is the Lifshitz-van der Waals free energy between the surface; r^{LW} is the Lifshitz-van der Waals component; the subscripts 1–3 represent the membrane, water and foulant, respectively; $\Delta G_{h_0}^{AB} = 2\sqrt{r_2^+}(\sqrt{r_1^-} + \sqrt{r_3^-} - \sqrt{r_2^-}) + 2\sqrt{r_2^-}(\sqrt{r_1^+} + \sqrt{r_3^+} - \sqrt{r_2^+}) - 2(\sqrt{r_1^+ r_3^-} - \sqrt{r_1^- r_3^+})$ is the acid-base free energy between solute and membrane surface at contact; his the separation distance; r^+ and r^- are the electron acceptor and electron donor component, respectively; λ is the decay length of *AB* interaction (λ = 0.6 nm) [25]; ε_r represents the dielectric constant of the bulk fluid (ε_r = 78.5 F/m); ε_0 is the permittivity of free space ($\varepsilon_0 = 8.854 * 10^{-12}$ F/m); ξ_1 and ξ_3 are the surface potentials of membrane and foulant, respectively; $\frac{1}{\kappa} = \sqrt{\varepsilon_0 \varepsilon_r R_g T / (2F^2 I_s)}$ represents the Debye length; R_g is the gas constant (R_g = 8.314J/(mol*K)); T is the absolute temperature in Kelvin; *F* represents the Faraday's constant (*F* = 96485C/mol); I_s is the ionic strength (I_s = 0.01 mol/L). All the parameters of surface tensions and zeta potential of foulants and membranes were measured in a 0.01 mol/L NaCl solution at pH 7.0 according to the method repoted by Zhang et al. [26].

According to the Young's equation [Eq. (6)], the parameters of r_i^{LW}, r_i^{AB} and r_i^{EL} (i = 1,3) can be calculated after measuring contact angle data (θ) for three probe liquids with known surface tension parameters(r_L^{LW}, r_L^+ and r_L^-). And the contact angle measurement was specifically conducted

using the Lifshitz-van der Waals acid-base (*LW-AB*) method, which was previously described by Sharma and Rao [27].

$$(r_L^{LW} + 2\sqrt{r_L^+ r_L^-})(1+\cos\theta) = 2(\sqrt{r_i^{LW} r_L^{LW}} + \sqrt{r_i^+ r_L^-} + \sqrt{r_i^- r_L^+}) \quad (6)$$

3. Results and discussions

3.1. Effect of Ca^{2+} on the changes of feed properties

3.1.1. Zeta potential changes

The charge property of feed (zeta potential) obviously changed as a result of the presence of Ca^{2+}, and the result is specifically presented in Table 1. Regardless of the feed composition, the zeta potential obviously decreased with a trend towards the neutral state upon the presence of Ca^{2+}.

a. BSA
   The zeta potential of BSA solution changed from –11.33 to –16.80 mV after 75°C heating, which might be associated with the conformational changes of BSA molecules (Supplementary S1) during the feed heating process [28]. The negatively charged groups of thermal-denatured BSA were unfolded to the molecular surface, resulting in an increase of zeta potential. Upon the addition of Ca^{2+}, the zeta potential of BSA solution significantly decreased from –16.80 to –4.06 mV. It might be due to that the negatively charged groups on the BSA molecular surface could be easily screened by the counter-ions Ca^{2+}, leading to an obvious decrement of zeta potential.
b. LYS
   Different from BSA, the LYS was positively charged (ξ = 6.88 mV) at the room temperature, while its zeta potential distinctly decreased to –14.10 mV during the feed heating process. As shown in Supplementary S1, nearly no conformational change was observed for LYS after 75°C heating, thus the obvious decrement of zeta potential might be attributed to the change of its *IEP*. As Bjellqvist et al. [29] reported, the *IEP* of proteins was partly affected by the temperature, which would decrease to a certain degree during the feed heating process. As shown in Fig. 1, the *IEP* of LYS significantly changed from 11.35 to 6.87 after 75°C feed heating, whereas that of BSA was nearly invariable with a range of 4.7–5.6. This suggested that the free carboxyl groups on the terminal of LYS as well as the side-chain carboxyl groups partly dissociated into the negatively charged $–COO^-$, leading to the distinct decrement of zeta potential. Furthermore, the zeta potential of LYS solution obviously decreased from –14.10 to –1.43 mV with the presence of Ca^{2+}, which was highly associated with the electrostatic attraction between LYS and Ca^{2+}. The Ca^{2+} could be interacted with the negatively charged $–COO^-$ of heated LYS molecules. The interaction between Ca^{2+} and $–COO^-$groups finally caused an obvious decline of zeta potential of LYS with a trend towards the neutral.
c. SA
   The zeta potential of SA solution obviously changed from –76.80 to –50.60 mV during the feed heating process, which might be due to the conformational changes of SA (Supplementary S1). Upon the addition of Ca^{2+}, the zeta potential greatly decreased to –11.20 mV. As shown in Table 1, when $Ca^{2+}$was added, the most significant change of zeta potential was observed for SA compared to BSA and LYS, which was mainly attributed to the obvious bridging effect between SA chains and Ca^{2+}. The divalent Ca^{2+} was largely cross-linked with the carboxylate groups of poly-L--guluronate (poly-G) residues in SA molecules [30], leading to the formation of nearly neutral gel-like complexes.
d. Mixed feed containing BSA (or LYS) and SA
   Noticeably, a relatively sever decline of zeta potential was observed for the mixed feed (BSA/SA or LYS/SA) in comparison with the individual feed solution.

The zeta potential of BSA/SA mixed feed exhibited a decrement from –74.20 to –47.10 mV after 75°C feed heating. Upon the presence of Ca^{2+} in BSA/SA solution, the zeta potential further decreased to –8.70 mV, which was mainly associated with the synergy effect between BSA, SA

Table 1
Detail characteristics of the organic feed solutions

Feed solution	Foulant composition ratio	pH	Zeta potential ξ (mV) (1)	Zeta potential ξ (mV) (2)	Zeta potential ξ (mV) (3)	Particle size (nm) (1)	Particle size (nm) (2)	Particle size (nm) (3)
BSA	100%	7.00±0.20	–11.33±1.76	–16.80±1.91	–4.06±0.91	71.4±1.3	102.9±1.2	122.4±2.0
LYS	100%	7.00±0.20	6.88±1.37	–14.10±1.22	–1.43±0.53	22.7±1.1	35.4±1.7	37.8±1.4
SA	100%	7.00±0.20	–76.80±3.13	–50.60±3.01	–11.20±1.21	162.1±2.4	109.6±2.2	198.4±2.6
BSA+SA	50% + 50%	7.00±0.20	–74.20±1.86	–47.10±2.78	–8.70±0.99	\	122.1±2.3	8983.4±13.8
LYS+SA	50% + 50%	7.00±0.20	–61.30±1.77	–46.00±2.66	–5.75±0.98		235.6±3.1	6549.1±9.4

1 The zeta potential (or particle size) of feed containing no Ca^{2+} was measured under the room temperature.
2 The zeta potential (or particle size) of feed containing no Ca^{2+} was measured after 75°C heating.
3 The zeta potential (or particle size) of feed containing Ca^{2+} was measured after 75°C heating.

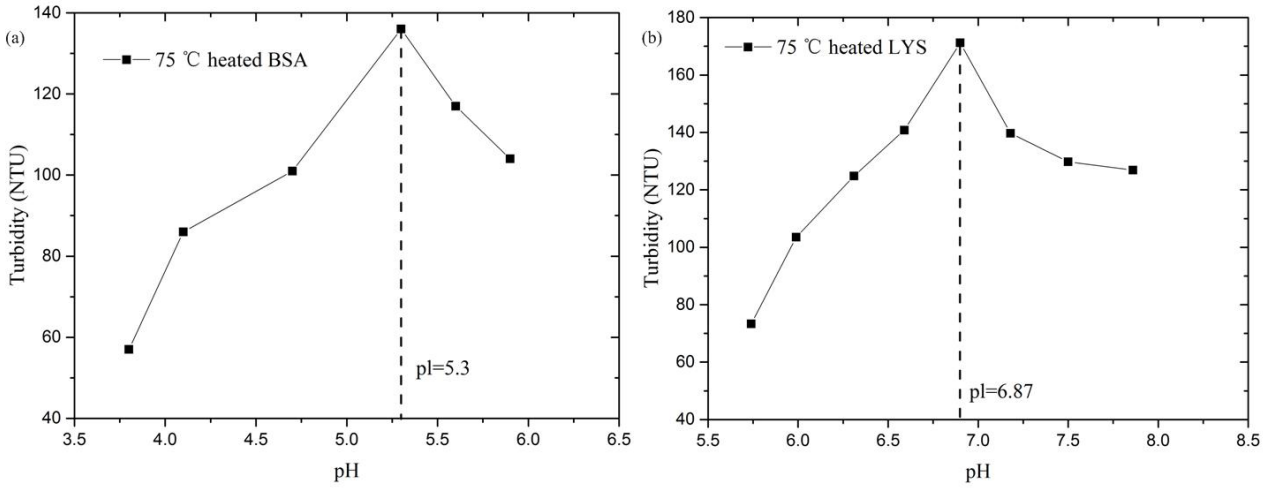

Fig. 1. Time dependency of measured turbidity of 75°C heated feed solution. (a) BSA solution; (b) LYS solution;

and Ca^{2+}. Similarly, the zeta potential of LYS/SA solution decreased from –61.30 to –46.00 mV during the feed heating process, and then changed to –5.75 mV with the addition of Ca^{2+}. It might be due to that more Ca^{2+} could be bound to SA chains compared to LYS, leading to a greater decrement of zeta potential for LYS/SA solution.

3.1.2. Particle size changes

In order to further investigate the binding mechanism between Ca^{2+} and different organics, zetasizer measurement was applied to study the size changes of feed with the addition of Ca^{2+}. The influence of Ca^{2+} on particle size of feed is displayed in detail in Table 1. It can be obviously observed that the particle size of feed significantly changed due to the presence of Ca^{2+}.

a. BSA
   As presented in Table 1, the particle size of BSA obviously increased from 71.4 to 102.9 nm after 75°C feed heating, which was highly attributed to the conformation changes of BSA. The hydrophobic residues of thermal-denatured BSA molecules were unfolded to the molecular surface, strengthening the aggregation between BSA molecules. Additionally, the particle size of BSA further increased to 122.4 nm with the addition of Ca^{2+}, which was mainly due to the binding affection between BSA molecules and Ca^{2+}. Ca^{2+}could be bound to the binding sites of BSA (such as free carboxyl groups), and formed the Ca-BSA complexes [31], leading to the increment of particle size. Furthermore, the negatively charged residues (such as sulphydryl) of thermal-denatured BSA [32] were largely screened by the counter-ions Ca^{2+}, further accelerating the aggregation of BSA molecules.
b. LYS
   Different from BSA, the particle size of LYS solution was almost unchanged, which only increased from 22.7 to 35.4 nm during the heating process. With the addition of Ca^{2+} in LYS solution, the particle size slightly changed to 37.8 nm. It was highly associated with the enhanced thermal stability of LYS that induced by Ca^{2+} [33]. Additionally, different from the BSA, there was no binding site for the native egg-white LYS to combine with Ca^{2+} [34]. The Ca^{2+} was just interacted with LYS through the electrostatic attraction, which was hard to form the complexes. Therefore, rather small changes were obtained for the particle size of LYS.
c. SA
   Different from BSA and LYS, the particle size of SA significantly decreased from 162.1 to 109.6 nm after 75°C heating. During the heat treatment, the depolymerization of SA was occurred through the breaking of the β-1,4-glycosidic bond [35], hence the long-chain SA molecules were partly depolymerized to a series of oligosaccharides, resulting in the obvious decrement of particle size. However, the particle size of SA significantly increased from 109.6 to 198.4 nm as the presence of Ca^{2+}, which was mainly associated with the bridging affection between Ca^{2+} and SA chains. Large amount of Ca^{2+} was cross-linked with the $–COO^-$ of poly-L--guluronate (poly-G) residues in SA molecules [30], leading to the formation of a highly compacted egg-box-shaped gel network [36]. The Ca^{2+} led to the firmer binding between different SA chains and then the further package of "box" around the "eggs", finally resulting in the formation of macromolecular gel-like "SA-Ca^{2+}" complexes.
d. Mixed feed containing BSA (or LYS) and SA
   The particle size of mixed feed significantly changed with the addition of Ca^{2+}. As shown in Table 1, the particle size of BSA/SA increased from 122.1 to 8983.4 nm, and that of LYS/SA changed from 235.6 to 6549.1 nm upon the presence of Ca^{2+} in feed solution.

For the mixed feed without Ca^{2+}, the particle size of LYS/SA (235.6 nm) was generally larger than that of BSA/SA (122.1 nm). It might be due to that the LYS was mainly linked with the poly-D-mannuronate (poly-M) residues of SA molecules, and partly bound to the $–COO^-$ of G residues [30], resulting in a relatively stronger complexation between LYS and SA molecules. Without the binding effection that Ca^{2+} played, a weaker complexation was obtained between BSA and SA, causing a lower particle size for BSA/SA solution.

Conversely, the particle size of LYS/SA solution (8983.4 nm) was obviously lower than that of BSA/SA (6549.1 nm) with the addition of Ca^{2+}. It was attributed to the synergy between BSA, SA and Ca^{2+}, partly strengthening the complexation between BSA and SA, while the complexation of LYS/SA was quite weakened due to competition between LYS and Ca^{2+} for the $–COO^-$ of G residues.

3.2. Effect of Ca^{2+} on membrane fouling rate

3.2.1. Permeate flux changes

The effect of Ca^{2+} on flux behavior is well presented in Fig. 2, which showed that the presence of Ca^{2+} in the feed solution would partly aggravate the fouling rate.

a. BSA

As displayed in Table 1, the presence of Ca^{2+} in BSA solution caused obvious changes of zeta potential and particle size, while only slight difference was observed for the flux decline behavior of BSA. The *NF* in the absence of Ca^{2+} slowly decreased to 0.90 upon the first two days, and then approximately reduced to 0.67 with a faster speed. With the addition of Ca^{2+}, the obvious flux decline for BSA lately started from the third day, and finally decreased to about 0.61.

Based on the final value of *NF*, it can be concluded that the flux decline behavior of BSA solution slightly became severe as the addition of Ca^{2+}, which was mainly due to the interaction between Ca^{2+} and BSA. The formation of "BSA-Ca^{2+}" complexes, the decreasing zeta potential as well as the increasing hydrophobicity induced the aggregation and deposition of BSA molecules on the membrane surface, finally causing a relatively serious membrane fouling.

b. LYS

Different from BSA, a rather obvious change was observed for the flux decline behavior of LYS with the presence of Ca^{2+}. The *NF* of pure LYS rapidly decreased to 0.75 upon the first day, and then approximately decreased to 0.55 with a relatively slower speed. In contrast, the *NF* with the presence of Ca^{2+} decreased rapidly all through the operation process, and the final *NF* was around 0.35. The significant flux decline behavior for LYS solution containing Ca^{2+} was associated with its nearly neutral zeta potential and small particle size. The nearly neutral LYS with small particle size was easily attached onto the membrane surface or even penetrated into the pores (Supplementary S2), resulting in a rapid membrane fouling rate.

c. SA

As shown in Fig. 2, the flux decline behavior of SA was also affected by the presence of Ca^{2+}. The *NF* in the absence of Ca^{2+}obviously decreased to 0.73 on the first day, and then slowly decreased to 0.60 at later stage. Upon the addition of Ca^{2+}, the *NF* rapidly decreased to 0.66 within 0.5 d, and then tardily decreased to around 0.50 in the end.

Additionally, the flux for SA finally reached a relatively stable state at later stage regardless of the presence of Ca^{2+}, which was highly associated with the formation of a gel layer on the membrane surface. Without the binding effect ion that Ca^{2+} played, the SA molecules could also form a gel-like

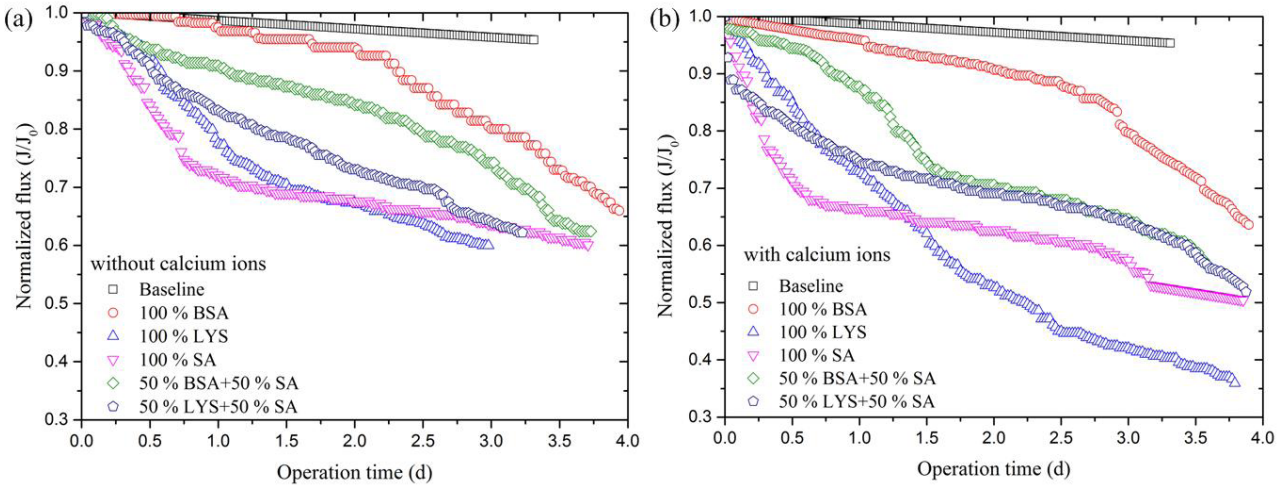

Fig. 2. Effect of Ca^{2+} on MD flux decline behavior. (a) feed solution without Ca^{2+}; (b) feed solution with Ca^{2+}; (Test condition: total organics concentration of 150 mg/L,10 mM$CaCl_2$, pH 7, and temperature difference of 75–15°C)

layer on the membrane, and this interesting phenomenon could be well interpreted by the "Clusters Theory" [37]. With the increment of SA concentration in feed side, the SA polymer chains would be collided with each other, and finally form a gel network due to the higher intermolecular forces such as hydrogen bonding force. Therefore, the SA solution could also form a gel layer on the membrane surface during the concentration process of feed, while that gel layer was much milder than the "SA-Ca^{2+}" gel deposition [4]. Comparatively, Ca^{2+} would be largely cross-linked with the $–COO^-$ groups of SA in a highly organized manner [30], leading to a firmer binding between different SA chains as well as the formation of a highly compacted "egg-box-shaped gel network" [38].

As a whole, the membrane fouling was much severe as the SA solution containing Ca^{2+}, which was due to the fast formation of a dense and firm gel-like layer that caused by the bridging between Ca^{2+} and SA molecules.

d. Mixed feed containing BSA (or LYS) and SA

The flux decline behavior of mixed feed significantly changed with the addition of Ca^{2+}. When the mixed feed contained Ca^{2+}, the flux decline behavior was relatively severe than that of protein at early stage, and then more tended to that of SA at later stage of MD operation. For example, the *NF* of 50% BSA in the presence of Ca^{2+} rapidly reduced to 0.70 at early stage (0–1.5 d), and then slowly decreased to 0.50 (the 4th day) with a decline trend similar to that of 100% SA. It might be associated with the formation of a firm and dense"SA-Ca^{2+}-protein" gel layer at later stage. A period of time was essential for the complete formation of that gel-like layer on the membrane surface. Hence, the nearly neutral proteins (BSA or LYS molecules) could largely attach onto the membrane surface or partly penetrate into the pores at early stage, resulting in a faster flux decline trend compared to the mixed feed containing no Ca^{2+}. With the gradual formation of a firm and stable "SA-Ca^{2+}-protein" gel layer on the membrane surface, the proteins were largely intercepted outside the pores, causing anobvious decrement of fouling rate.

However, the flux decline behavior of mixed feed containing no Ca^{2+} was rather similar to that of BSA or LYS all through the MD process. For example, the *NF* of BSA/SA finally decreased to around 0.60 with a decline trend similar to that of sure BSA. This phenomenon might be due to that small amounts of SA monomers with the absence of Ca^{2+} was unable to form a firm gel network, thus the proteins would obviously attach onto the membrane surface and penetrate into the pores, leading to a flux decline similar to that of proteins. Compared to BSA/SA, the LYS/SA solution caused a relatively severe flux decline behavior as a result of the lower particle size of LYS (35.4 nm).

3.2.2. SEM analysis of membrane

To further investigate the effect of Ca^{2+} on the membrane fouling, the SEM-EDX analysis was adopted to quantify the organic contents on the membrane (Fig. 3). On the basis of the elements composition of organics [39], the carbon (C) and oxygen (O) elements were chosen as the representative elements for the deposited organic mass.

a. Morphology of membrane surface

The surface micromorphology of fouling layer displayed significant differences, which is intuitively presented in Fig. 3. The most obvious difference was observed for the SA fouled membranes (Figs. 3c,h). The fouling layer caused by pure SA solution presented a nubbly form (Fig. 3c), while that was bacilli form with the addition of Ca^{2+} in SA solution (Fig. 3h). The deposit layer of BSA and LYS both exhibited a nubbly morphology regardless of the presence of Ca^{2+}. Furthermore, lower porosity was observed for the fouling layer as the feed solution containing no Ca^{2+}, which was partly due to its lower particle size.

b. Intensity changes of deposited organic mass

Except the surface morphology, obvious changes were also obtained for the intensity of organic mass with the presence of Ca^{2+}. The EDX analysis of fouled membranes by different organics is well presented in Fig. 3. The fouled membrane by LYS displayed the most significant intensity for organic residues (C and O element). It might be due to the lowest particle size and the weakest electrostatic repulsion from the negative membrane surface in comparison with BSA and SA. Additionally, the lowest organic mass deposition was observed for the SA as a result of its extremely high hydrophilicity, although a rather severe flux decline was indeed obtained for SA solution.

With the presence of Ca^{2+}, obvious increment of organic mass was observed on the fouled membrane surface. For example, the total intensity of organic residues (C element and O element) obviously increased from 7.55 to 13.28 CPS/keV with the addition of Ca^{2+} in SA solution. It was mainly attributed to the cross-linking between Ca^{2+} and SA (marked with red cycle in Fig. 3h), leading to the continuous package of "egg-box" [38]. Additionally, the intensity of organic residues significantly increased from 8.97 to 16.82 CPS/keV when the Ca^{2+} was added into the BSA solution. It was highly associated with the largely aggregation and deposition of BSA that induced by Ca^{2+}. In constant, the total intensity of organic residues slightly increased from 29.10 to 33.06 CPS/keV with the presence of Ca^{2+} in LYS solution. Conclusively, upon the addition of Ca^{2+}, more obvious changes of organic mass were observed for the BSA as well as the SA, while the least change was for the LYS. It can be explained by the fact that Ca^{2+} could be significantly bound with BSA and SA, whereas that just weakly interacted with LYS through the electrostatic attraction. However, more significant changes of flux decline behavior were observed for LYS upon the addition of Ca^{2+}. It might be due to that the BSA and SA molecules were mainly deposited onto the membrane sur-

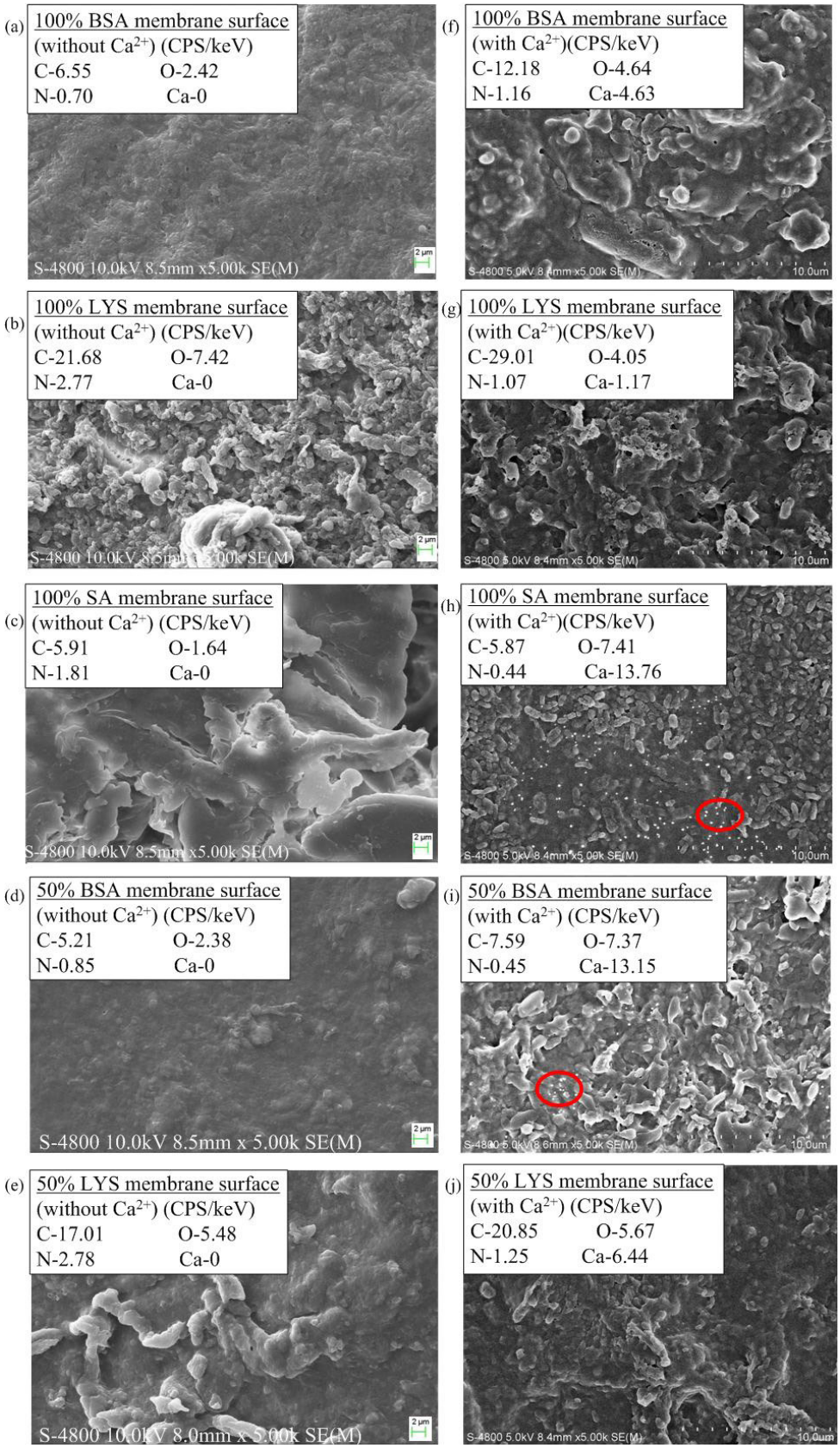

Fig. 3. SEM-EDX membrane surface analysis of fouled membranes. (a)–(e) feed solution without Ca^{2+}; (f)–(j) feed solution containing Ca^{2+}.

face, while LYS molecules could largely penetrate into the pores except the membrane surface (Supplementary S2). As Tijing et al. [5] reported, the pore blocking fouling was irreversible and could cause more serious membrane degradation than the external surface fouling. Therefore, more severe flux decline was observed for LYS with the presence of Ca^{2+}, which was mainly associated with the increasing pore blocking phenomenon.

Additionally, the EDX analysis of fouled membranes by mixed feed solutions is also demonstrated in Fig. 3. With the addition of Ca^{2+}, the organic mass on the membrane surface both increased, and 50% BSA displayed a more significant increment. The total intensity of organic mass (C and O element) obviously increased from 7.59 to 14.96 CPS/keV with the presence of Ca^{2+} in 50% BSA solution. It was highly due to the synergic effect among BSA, Ca^{2+} and SA during the continuous formation of a dense and firm "SA-Ca^{2+}-BSA" gel-like layer (marked with red cycle in Fig. 3i) [40], resulting in a large amount of mass deposition and then aggravating the membrane fouling. The Ca^{2+} was cross-linked with the $–COO^-$ of poly-L-guluronate (poly-G) residues in SA molecules [30], leading to the formation of a gel-like layer. Furthermore, BSA molecules played an enhanced role in the formation of that gel-like deposit layer, consequently strengthening the cross-linking effect and then accelerating the attachment rate. Additionally, the intensity of organic residues slightly increased from 22.49 to 26.52 CPS/keV with the addition of Ca^{2+} in 50% LYS solution, which was mainly attributed to the obvious decrement of zeta potential. Ca^{2+} significantly competed with the negatively charged LYS for the G residues, thus the LYS molecule largely fell off the SA chains [30]. Fraction of LYS were still linked to the poly-D-mannuronate (poly-M) residues with a weaker binding force, partly promoting the pairing of the monocomplexes (Ca^{2+}-single guluronate unit). Therefore, the increment of mass deposition induced by the presence of Ca^{2+} wasn't so obvious in comparison with the 50% BSA mixed feed.

3.3. Correlation between fouling behavior and foulant-membrane interaction energy

Organic fouling process was confirmed to be controlled by the foulant-membrane and foulant-foulant interactions [41], and the inclusive EL, LW and AB interaction could be well predicted by the XDLVO theory. The interfacial energy between feed and PTFE membrane surface was well calculated through the XDLVO model [42,43], and the corresponding profiles for the energy versus distance are intuitively presented in Fig. 4, Fig. 5 and Supplementary S3.

During the initial period of membrane fouling, the deposition of foulants onto the MD membrane was mainly influenced by the interfacial interaction energy between foulants and membrane surface. As shown in Figs. 4 and 5, an energy barrier was observed from the interaction energy profiles for the feed in the absence of Ca^{2+}. The energy barrier, which was the maximum repulsion energy, partly suggested that the feed should have sufficient kinetic energy to overcome this barrier towards the membrane surface [44]. The energy barriers for BSA, LYS and SA were 73.86, 22.77 and 227.81 kT, respectively. In general, lower energy barrier would cause a faster and severe membrane fouling behavior (LYS). However, SA displayed a more serious flux decline behavior than BSA in spite of its higher energy barrier, which might be due to the formation of a dense gel layer on the membrane surface. Additionally, the presence of SA in mixed feed largely increased its energy barrier, which was 276.25 and 520.74 kT for 50% BSA and 50% LYS, respectively. Despite of the rather higher energy barrier, mixed feed still presented a relatively severe fouling behavior than BSA. Part of protein molecules would penetrate into the pores in the form of monomers. On the other hand, some proteins would combine with SA and form the "SA-protein complexes". The "SA-protein complexes" continuously deposited onto the membrane surface, leading to the formation of a relatively dense fouling layer. Therefore, the mixed feed with higher energy barrier still displayed a rather serious flux decline behavior instead in comparison with BSA solution.

With the addition of Ca^{2+} in the feed solution, the energy barrier of feed significantly decreased to a rather lower value, indicating that the organics were easier to be attached onto the membrane surface and ultimately caused a rather serious flux decline. For example, the energy barrier for 100% SA, 50% BSA and 50% LYS significantly decreased from 227.81, 276.25 and 520.74 kT to 16.88, 1.99 and 1.01 kT, respectively. Furthermore, the energy barrier of 100% BSA and 100% LYS both magically disappeared upon the presence of Ca^{2+}, and its total interaction became attractive. The significant change was highly associated with the distinct interaction mechanism between Ca^{2+} and different feeds which were detailedly discussed in section 3.4.

Additionally, the change trend of interaction energy along with the separation distance was largely affected by the presence of Ca^{2+}. As a whole, the attractive AB interactions between foulants (without Ca^{2+}) and membrane surface were dominated at short separation distance (SSD), and the total interaction was attractive. For example, the SSD were 0–2.5, 0–3.0 and 0–1.5 nm for 100% BSA, 100% LYS and 100% SA, respectively. With the further increment of separation distance, the repulsive EL interaction was dominated and the total interaction quickly became repulsive. With the presence of Ca^{2+} in feed solution, the EL interaction energy obviously reduced as a result of the distinct decline of zeta potential of feed, while nearly no changes were observed for the AB and LW interaction. For example, at 1.0 nm, the EL interaction energy between BSA and membrane significantly decreased from 131.93 to 7.17 kT. The EL interaction between LYS and membrane completely changed from repulsive to attractive with the addition of Ca^{2+}. Eventually, the total interaction (100% BSA or 100% LYS) significantly changed from repulsive to attractive due to the decrement of the main repulsive interaction-EL interaction, ultimately resulting in a distinct aggravation of membrane fouling. Different from 100% BSA and 100% LYS, the energy barrier still existed for the 100% SA with Ca^{2+}, and a secondary energy minimum (the maximum attraction energy) of –6.30 kT also existed, which represented the ability of SA being sucked onto the membrane surface [45].

Comparatively, the most significant changes of interfacial energy were observed for the mixed feed with the addition of Ca^{2+}. In terms of the 50% BSA, the AB interaction was dominated at 0–2.0 nm, while that was dominated at 0–4.5 nm separation distance with the presence of Ca^{2+}. The

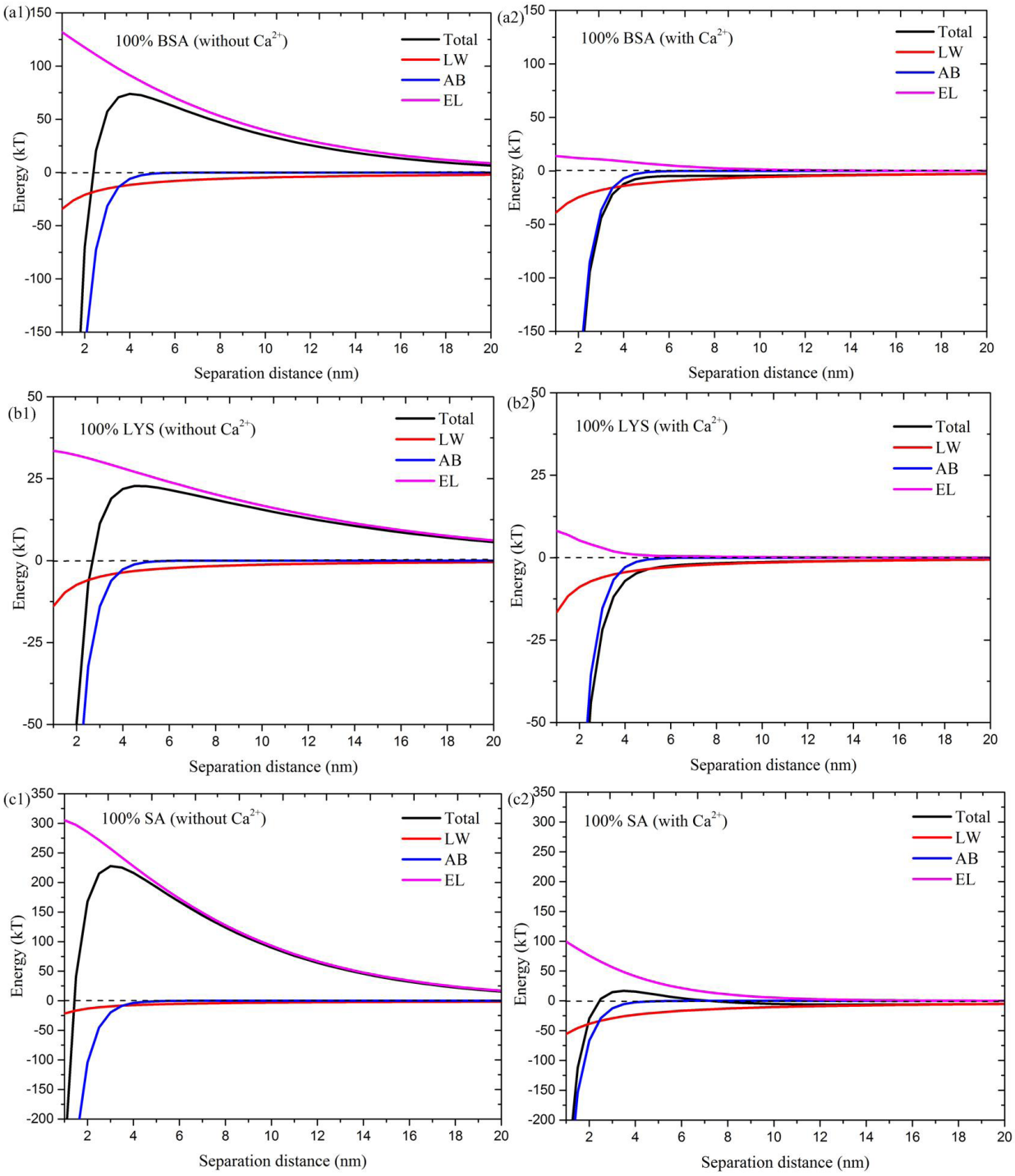

Fig. 4. Interaction energies profiles between each individual foulant and membrane as a function of separation distance: (a) 100% BSA; (b) 100% %LYS; (c) 100% SA;

EL interaction energy between 50% BSA and membrane obviously reduced from 344.45 (1.0 nm) to 35.50 kT with the addition of Ca^{2+}. Regarding the 50% LYS, the AB interaction was dominated at 0–1.0 nm, whereas that was dominated at 0–4.5 nm as the addition of Ca^{2+}. The EL interaction energy between 50% LYS and membrane magically decreased from 615.13 (1.0 nm) to 9.36 kT with the presence of Ca^{2+}. The significant decrement of EL interaction energy obviously caused a noteworthy decline of the total interaction, ultimately leading to an obvious aggravation of membrane fouling with the addition of Ca^{2+}. Additionally, the maximum attractive energies (secondary energy minimum) also existed for mixed feed in the presence of Ca^{2+}, which were –2.59 and –0.46 kT for 50% BSA and 50% LYS, respectively,

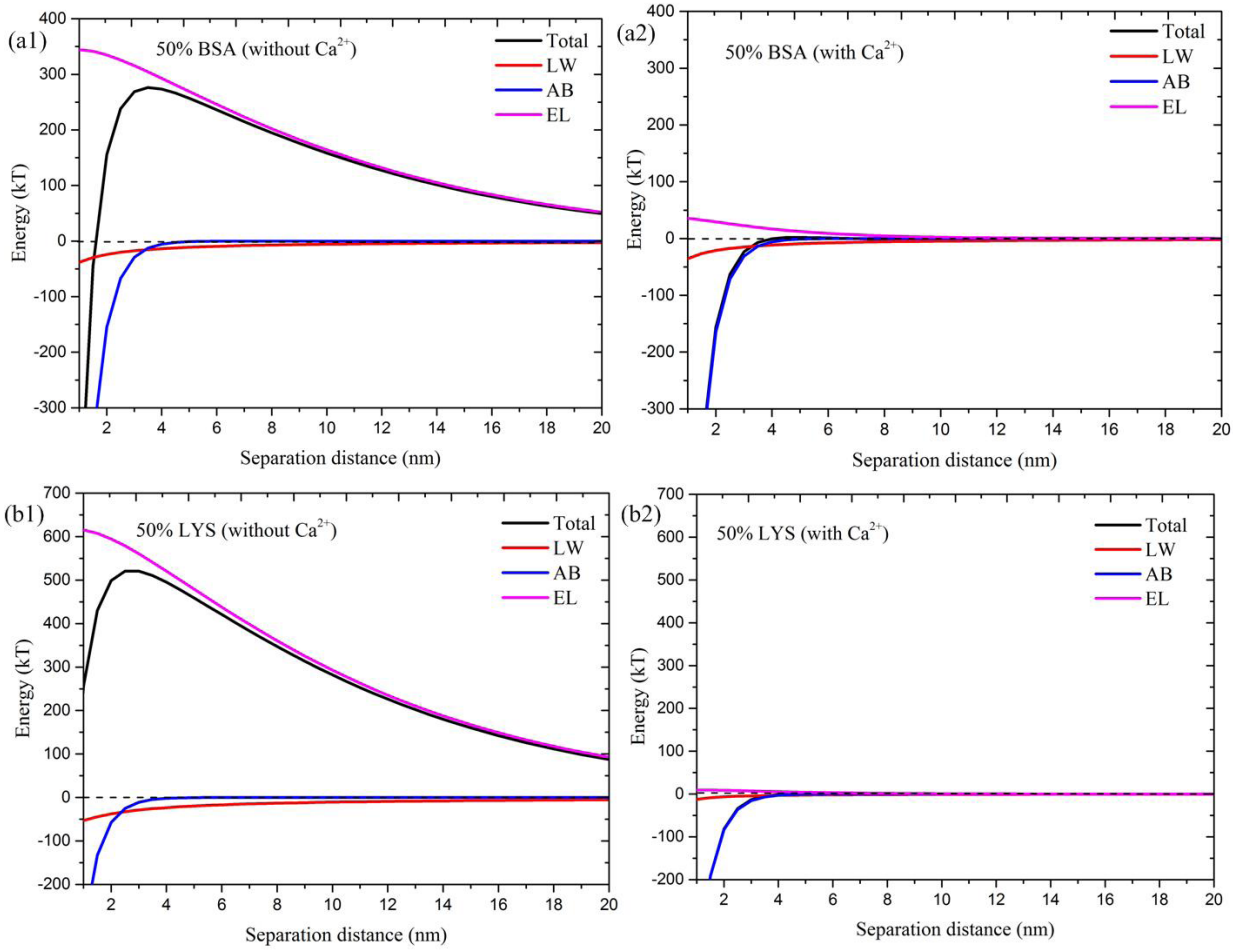

Fig. 5. Interaction energies profiles between mixed foulants and membrane as a function of separation distance: (a) 50% BSA+50% SA; (b) 50% LYS+50% SA;

showing the ability of 50% BSA or 50% LYS being sucked onto membrane surface.

At the later stage, the membrane surface was nearly covered by a foulant deposit layer, the subsequent and long-term foulant deposition was largely governed by the foulant-foulant interfacial interactions. The interaction energies between foulants in bulk solution and foulants on MD membrane surface (i.e., in the fouling layer) were calculated, and the corresponding interfacial interaction energy profiles are presented in Supplementary S3. The shape of these interaction energy curves of foulant-foulant was a bit different from that of foulant-membrane. The foulant particle encountered a weak attraction at a distance of about 20–30 nm due to the presence of the *LW* attraction. Then the total interaction became repulsion as the foulant particle approached to the fouled membrane surface, which was highly attributed to the dominant *AB* repulsion and *EL* repulsion. This repulsion between foulants and deposited fouling layer was maximum when the foulant particle contacted the fouled MD membrane surface. As reported by Ding et. al [46], the foulant particle was easier to continuously deposit onto the fouled MD membrane when the distance (critical distance) from fouling layer on MD membrane surface to the critical point (the point where no repulsion energy was observed) was shorter. As shown in Supplementary S3, the critical distance of SA (23.0 nm) was obviously longer than that of BSA (10.0 nm) and LYS (9.0 nm), further confirming the lower amount of SA molecules on the MD membrane surface (Supplementary S2). With the addition of Ca^{2+} in feed solution, the critical distance of foulant-foulant was obviously decreased regardless of the types of foulants. As exhibited in Supplementary S3, the critical distance of 100% BSA, 100% LYS, 100% SA, 50% BSA and 50% LYS distinctly decreased to 4.0, 3.5, 4.5, 3.0 and 2.5 nm, respectively. Therefore, it can be concluded that the interaction energies among foulant molecules and between foulant molecules and MD membranes would obviously increase with the presence of Ca^{2+} in feed solution, significantly promoting the continuous deposition of foulants onto MD membrane surface.

3.4. Organic fouling behavior of MD in the absence and presence of Ca^{2+}

To gain further insight into the intermolecular interaction among different foulants and the effect of Ca^{2+} on organic fouling behavior, GPC has been proved to be an

effective and alternative method to investigate the formation mechanism of protein-Ca^{2+}-SA complexes [28]. And the correspondingly GPC profiles are well presented in Fig. 6 and Fig. 7.

Fig. 6a compares the different chromatograms of BSA with and without Ca^{2+}. As shown in Fig. 6a, the native BSA exhibited two major peaks at the evolution time of 11.291 and 11.473 min due to the dimeric and trimeric forms of BSA, as well as some fragments appeared at the evolution time of 13.731 min, which might be attributed to the small amount of BSA monomers. It can be surmised that the BSA solution in the absence of Ca^{2+} was mainly composed of water-soluble aggregates, and a handful of BSA monomers. This result might be due to that the BSA molecules underwent conformational changes under the heating condition, resulting in the exposure of hydrophobic residues. The increased hydrophobicity would promote the aggregation of BSA molecules, leading to the formation of BSA aggregates. With the addition of Ca^{2+}, the evaluation time for the two major peaks shifted to 9.985 and 10.647 min, which might be associated with the screen effect that counter-ions Ca^{2+} played. The negatively charged residues which were exposed in the thermal condition, would be effectively screened by Ca^{2+}, leading to a distinct decline of zeta potential. The reduction of electrostatic repulsion significantly promoted the formation of large, non-soluble aggregates, and simultaneously expedited the deposition of BSA aggregates on the MD membrane surface, causing a relatively faster and sever flux decline.

Fig. 6b exhibited a similar chromatogram of LYS with the absence and presence of Ca^{2+}. The native LYS showed a major peak at the evolution time of 10.813 min, along with a minor peak at the evolution time of 12.361 min. With the addition of Ca^{2+} in LYS solution, the inspection of GPC profile revealed that nearly no change was observed for the evolution time of the major peak (10.836 min). This result confirmed that LYS was a kind of thermal-stable protein, and no conformational change was conducted under the heating condition. Ca^{2+} was just interacted with LYS molecules via the electrostatic attraction, thus the particle size of LYS was nearly unchanged. However, the LYS solution containing Ca^{2+} could significantly cause a faster and rather severe flux decline behavior, which was highly attributed to the obvious decline of zeta potential. The decrease of electrostatic repulsion partly promoted the deposition of LYS molecules on the membrane surface, leading to the formation of a thick and stable LYS fouling layer. Additionally, the rather lower particle size of LYS, partly promoting the obvious penetration of LYS molecules into membrane pores, thus caused an extremely faster flux decline.

Compared to the protein-like substances (BSA and LYS), obvious differences were observed from the chromatograms of SA in the absence and presence of Ca^{2+}. SA as a natural polysaccharide, is known to have a broad molecular mass distribution [47]. Fig. 6c shows the effect of Ca^{2+} on the chromatograms of SA. As can be observed, the native SA exhibited a major peak at the evolution time of 11.251 min due to the oligosaccharides form, along with a broad minor peak attributed to its long-chain molecules at the evolution time of 8.681~10.659 min. This distribution might be associated with the conformational changes of SA molecules in the thermal condition. As a previous research [35] reported,

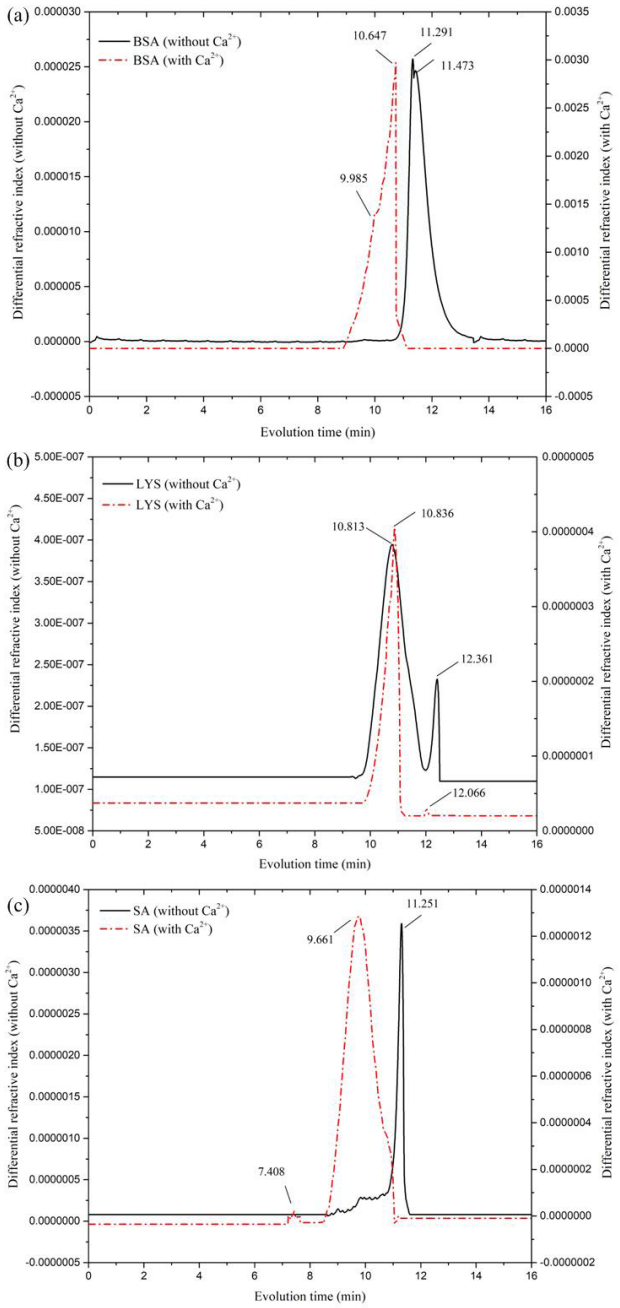

Fig. 6. GPC profiles of each individual foulant in the absence and presence of Ca^{2+}. (a) individual BSA solution; (b) individual LYS solution; (c) individual SA solution; (Testing condition: feed concentration of 150 mg/L, 10 mM $CaCl_2$, pH 7, and the individual solution was 75°C heated for 4d).

the depolymerization of SA occurred with heat treatment, resulting in the breaking of the β-1,4-glycosidic bond. With the addition of Ca^{2+} in SA solution, the GPC profile exhibited a significant decrease of evolution times of the major peak as well as the minor peak, in which the major peak distinctly decreased to 9.661 min and the broad minor peak changed to a sharp peak at the evolution time of 7.408 min. The increment of molecular weight was highly attributed

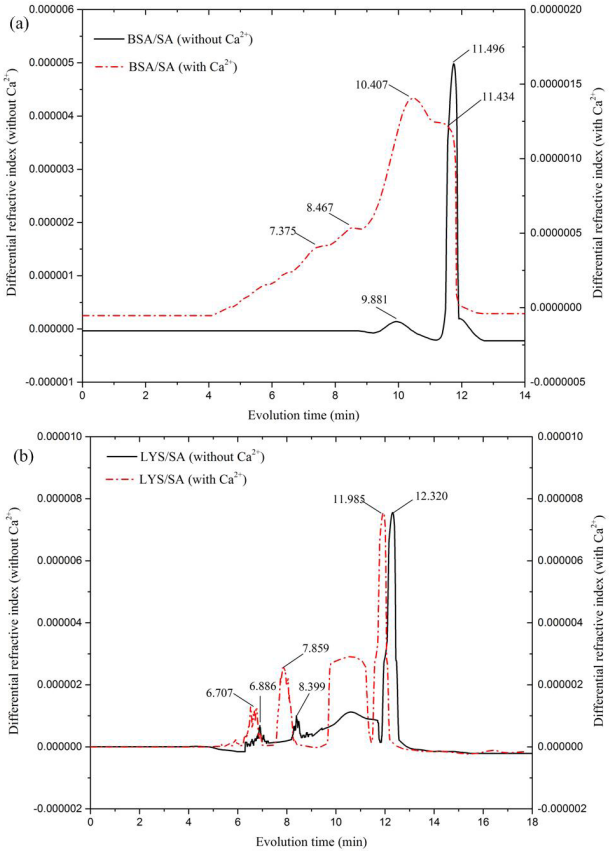

Fig. 7. GPC profiles of BSA/SA and LYS/SA mixture in the absence and presence of Ca^{2+}. (a) BSA/SA mixed solution; (b) LYS/SA mixed solution; (Testing condition: feed concentration of 150 mg/L, 10 mM $CaCl_2$, pH 7, and the mixed solution was 75°C heated for 4d).

to the continuous binding interactions between SA molecules and Ca^{2+}, leading to the large formation of macromolecular"SA-Ca^{2+}" complexes. The complexes would largely attach onto the membrane surface and then formed a dense gel layer, causing a rather faster and severe membrane fouling behavior than the native SA solution.

For the protein/SA mixtures, obvious changes were observed for the evolution time of peaks. As shown in Fig. 7 (a), the BSA/SA mixture in the absence of Ca^{2+} displayed two peaks at the evolution time of 11.496 and 9.881 min, representing the BSA and SA molecules. This result confirmed that nearly no intermolecular interaction between BSA and SA molecules was occurred. Therefore, the BSA/SA mixture in the absence of Ca^{2+} couldn't form a gel layer on the membrane surface, and large amounts of BSA molecules were attached onto the membrane surface or penetrated into the pores, resulting in a membrane fouling behavior similar to that for BSA alone. However, the GPC profile of BSA/SA mixture in the presence of Ca^{2+} was completely changed, revealed the important role that Ca^{2+} played in the formation of BSA-SA complexes. As can be seen, broaden-new peaks (4.182~11.615 min) appeared on the chromatograms were assigned as different sized BSA-Ca^{2+}-SA complexes, which was attributed to the long-chain molecules and oligosaccharides generated from the heated SA, as well as the large aggregates and segments resulting from the denatured BSA, suggesting the random occurrence of cross-linking interactions between BSA and SA molecules. The Ca^{2+} was cross-linked with the carboxylate groups of poly-L--guluronate (poly-G) residues in SA chains [30]. On the other hand, Ca^{2+} was bound to the negatively charged residues of denatured BSA molecules. Ca^{2+} served as a vinculum and bridge between BSA molecules and SA chains, leading to the formation of a dense and thick gel-like layer (BSA-Ca^{2+}-SA complexes) on the membrane surface, and correspondingly severe fouling behavior. Different from the BSA/SA mixture, the flux decline of BSA/SA/Ca^{2+} mixture slowed at the later stage, similar to what was obtained for SA/Ca^{2+}. It was highly associated with the complete formation of a new gel-like layer (BSA-Ca^{2+}-SA) at later stage, with mass and heat transfer resistance similar to that of the SA-Ca^{2+}.

The GPC profiles of LYS/SA mixture reveals the formation of larger LYS-SA complexes, indicated by the significant changes of peak shape and peak position. Except for the peaks of LYS (12.320 min) and SA (a broad peak of 9.422~11.243 min), the GPC profile of LYS/SA in the absence of Ca^{2+} showed two new peaks at the evolution time of 6.886 and 8.399 min, indicating the appearance of large "LYS-SA" complexes. As Fuenzalida et al. [30] reported, the LYS molecules could be linked with the poly-D-mannuronate (poly-M) residues of SA molecules as well as the $–COO^-$ of poly-L-guluronate (poly-G) residues in SA, resulting in the formation of "LYS-SA" complexes and correspondingly increased particle size. With the addition of Ca^{2+} in LYS/SA mixture, the GPC profile still exhibited a major peak at the evolution time of 11.985 min attributed to LYS monomers, and a broad peak (9.833~11.217 min) attributed to SA molecules. Additionally, two new peaks were observed at the evolution time of 6.707 and 7.859 min, which might be associated with the formation of "LYS-SA-Ca^{2+}" complexes. The Ca^{2+} could compact with LYS molecules for the Gresidues in SA chains [30], thus the LYS molecule largely fell off the SA chains and only a fraction of that was still linked to the M residues with a weaker binding force, partly promoting the pairing of the monocomplexes (Ca^{2+}-single guluronate unit). Similar to BSA/SA, the addition of Ca^{2+} in LYS/SA mixture also exhibited a slower flux decline behavior like SA alone at the later stage of MD operation, which was highly due to the formation of a stable gel-like layer (LYS-SA-Ca^{2+}) on the membrane surface.

As a whole, the presence of Ca^{2+} in feed solution would partly promote the organic fouling behavior during the MD operation. In terms of the individual feed solution, the most significant change was observed for SA with the addition of Ca^{2+}, which was highly attributed to the strong bridging between SA chains and Ca^{2+}. Besides, the denatured BSA molecules could also link with Ca^{2+} and then formed larger complex, leading to a more severe flux decline. In contrast, no linkage was obtained between Ca^{2+} and the thermal-stable LYS molecules for lack of binding sites. However, a significant flux decline could be observed with the presence of Ca^{2+}, which was mainly due to that the zeta potential of LYS obviously decreased to the nearly neutral level, resulting in an electrostatic induction between LYS molecules and membrane surface. With regards of the mixed feed solution, the Ca^{2+}played a decisive role in the formation of protein-SA complexes. The Ca^{2+} served as a vinculum and

bridge between denatured BSA molecules and SA chains, promoting the massive formation of a dense "BSA-Ca^{2+}-SA" gel layer on the membrane surface. Differently, the Ca^{2+} played a competition role during the intermolecular interaction between LYS and SA molecules. The Ca^{2+} could preferentially occupy its binding sites (G residues) in SA chains, and then the LYS molecules would largely fell off the SA chains. Small amount of LYS molecules still liked to the SA chains, and formed a thick LYS deposition layer containing several "LYS-SA-Ca^{2+}" gel-like layer. Therefore, most LYS molecules were intercepted outside the membrane pores, leading a milder fouling behavior than LYS alone. To summarize, the presence of Ca^{2+} in organic feed solution would partly interact with organic foulants, leading to the formation of protein-polysaccharide complexes and finally a faster and more severe flux decline.

4. Conclusions

In this study, the specific effect mechanism of Ca^{2+} during the organic fouling process of DCMD was systematically investigated using feed solutions with different organics compositions. The results led to the following conclusions:

1. The zeta potential of feed solutions all obviously decreased with the presence of Ca^{2+}, resulting in a decrease of electrostatic repulsion with the membrane surface and then a more severe fouling behavior. The mixed feed containing 50% BSA or 50% LYS displayed the most significant decrement of zeta potential, and then followed by 100% SA, 100% LYS.
2. Except for the LYS solution, the presence of Ca^{2+} in feed solution would significantly cause the formation of complexes, leading to the obvious increment of particle size. The formation of complexes partly promoted the deposition of fouling layer on the membrane surface, leading to a more serious flux decline.
3. The flux decline behavior of MD was partly changed as the addition of Ca^{2+} in feed solution. The most obvious change was observed for the mixed feed (BSA/SA or LYS/SA), which was extremely similar to that of protein (BSA or LYS) at early stage and then more tended to that of SA at later stage. It was highly due to the formation of a gel-like layer (protein-Ca^{2+}-SA) on the membrane surface, with a mass and heat transfer resistance similar to that of "SA-Ca^{2+}" gel layer.
4. With the presence of Ca^{2+} in feed solution, the EL interaction obviously decreased, whereas nearly no obvious changes were observed for the AB and LW interaction. The EL interaction even changed from repulsive to attractive, leading to a significant decrement of the total interaction energy and the corresponding sever membrane fouling. The energy barrier even disappeared with the presence of Ca^{2+} in BSA or LYS solution.
5. The effect degree of Ca^{2+} on different feed solutions was partly differed, which was highly associated with the interaction mechanism between Ca^{2+} and organics. The mixed feed (BSA/SA or LYS/SA) showed the most significant changes with the addition of Ca^{2+}, which might be due to the bond effect (or competition effect) that Ca^{2+} played between BSA (or LYS) and SA. Additionally, relatively distinct changes were also observed for the 100% SA and 100% BSA solution, whereas the least changes were observed for the 100% LYS solution.

Acknowledgements

This study was mainly financially supported by National Natural Science Fund of China (grant number: 51508153), Natural Science Fund of Jiangsu (grant number: BK20150813), Fundamental Research Funds for the Central Universities (grant number: 2018B15014), A Project Funded by the Priority Academic Program Development of Jiangsu Higher Education Institutions and Postgraduate Research & Practice Innovation Program of Jiangsu Province.

Reference

[1] J.G. Lynam, G.I. Chow, C.J. Coronella, S.R. Hiibel, Ionic liquid and water separation by membrane distillation, Chem. Eng. J., 288 (2016) 557–561.
[2] H.C. Kim, J. Shin, S. Won, J.Y. Lee, S.K. Maeng, K.G. Song, Membrane distillation combined with an anaerobic moving bed biofilm reactor for treating municipal wastewater, Water Res., 71 (2015) 97–106.
[3] B. Mi, M. Elimelech, Chemical and physical aspects of organic fouling of forward osmosis membranes, J. Membr. Sci., 320 (2008) 292–302.
[4] A. Seidel, M. Elimelech, Coupling between chemical and physical interactions in natural organic matter (NOM) fouling of nanofiltration membranes: implications for fouling control, J. Membr. Sci., 203 (2002) 245–255.
[5] L.D. Tijing, Y.C. Woo, J.-S. Choi, S. Lee, S.-H. Kim, H.K. Shon, Fouling and its control in membrane distillation—A review, J. Membr. Sci., 475 (2015) 215–244.
[6] L.D. Nghiem, T. Cath, A scaling mitigation approach during direct contact membrane distillation, Sep. Purif. Technol., 80 (2011) 315–322.
[7] M. Gryta, M. Tomaszewska, J. Grzechulska, A. Morawski, Membrane distillation of NaCl solution containing natural organic matter, J. Membr. Sci., 181 (2001) 279–287.
[8] Y.-N. Wang, C.Y. Tang, Nanofiltration membrane fouling by oppositely charged macromolecules: investigation on flux behavior, foulant mass deposition, and solute rejection, Environ. Sci. Technol., 45 (2011) 8941–8947.
[9] H. Huachang, P. Wei, Z. Meijia, C. Jianrong, H. Yiming, W. Fangyuan, W. Xuexiang, Y. Haiying, L. Hongjun, Thermodynamic analysis of membrane fouling in a submerged membrane bioreactor and its implications, Bioresource Technol., 146 (2013) 7–14.
[10] Q. Wang, Z. Wang, C. Zhu, X. Mei, Z. Wu, Assessment of SMP fouling by foulant-membrane interaction energy analysis, J. Membr. Sci., 446 (2013) 154–163.
[11] M. Zhang, W. Peng, J. Chen, Y. He, L. Ding, A. Wang, H. Lin, H. Hong, Y. Zhang, H. Yu, A new insight into membrane fouling mechanism in submerged membrane bioreactor: osmotic pressure during cake layer filtration, Water Res., 47 (2013) 2777–2786.

[12] C.J.V. Oss, Hydrophobicity of biosurfaces-Origin, quantitative determination and interaction energies, Colloids Surf., B, 5 (1995) 91–110.
[13] C.J.V. Oss, A. Docoslis, W. Wu, R.F. Giese, Influence of macroscopic and microscopic interactions on kinetic rate constants: I. Role of the extended DLVO theory in determining the kinetic adsorption constant of proteins in aqueous media, using von Smoluchowski's approach, Colloids Surf., B, 14 (1999) 99–104.
[14] J.A. Brant, A.E. Childress, Assessing short-range membrane-colloid interactions using surface energetics, J. Membr. Sci., 203 (2002) 257–273.
[15] F. Lei, X.F. Li, G.C. Du, C. Jian, Adsorption and fouling characterization of Klebsiella oxytoca to microfiltration membranes, Process Biochem., 44 (2009) 1289–1292.
[16] V.T. Nguyen, T.W. Chia, M.S. Turner, N. Fegan, G.A. Dykes, Quantification of acid-base interactions based on contact angle measurement allows XDLVO predictions to attachment of Campylobacter jejuni but not Salmonella, J. Microbiol. Methods, 86 (2011) 89–96.
[17] L. Wang, R. Miao, X. Wang, Y. Lv, X. Meng, Y. Yang, D. Huang, L. Feng, Z. Liu, K. Ju, Fouling behavior of typical organic foulants in polyvinylidene fluoride ultrafiltration membranes: characterization from microforces, Environ. Sci. Technol., 47 (2013) 3708–3714.
[18] M. Gryta, Fouling in direct contact membrane distillation process, J. Membr. Sci., 325 (2008) 383–394.
[19] Y. Shim, H.-J. Lee, S. Lee, S.-H. Moon, J. Cho, Effects of natural organic matter and ionic species on membrane surface charge, Environ. Sci. Technol., 36 (2002) 3864–3871.
[20] E.J. Cohn, L.E. Strong, W.L. Hughes, D.J. Mulford, J.N. Ashworth, M. Melin, H.L. Taylor, Preparation and properties of serum and plasma proteins. iv. a system for the separation into fractions of the protein and lipoprotein components of biological tissues and fluids, J. Am. Chem. Soc., 68 (1946) 459–475.
[21] O. Wintersteiner, H.A. Abramson, The isoelectric point of insulin: electrical properties of adsorbed and crystalline insulin, J. Biol. Chem., 99 (1933) 741–753.
[22] K. Xiao, X. Wang, X. Huang, T.D. Waite, X. Wen, Combined effect of membrane and foulant hydrophobicity and surface charge on adsorptive fouling during microfiltration, J. Membr. Sci., 373 (2011) 140–151.
[23] A.F. Stalder, G. Kulik, D. Sage, L. Barbieri, P. Hoffmann, A snake-based approach to accurate determination of both contact points and contact angles, Colloids Surf. A, 286 (2006) 92–103.
[24] J.M. Meinders, H.C.V.D. Mei, H.J. Busscher, Deposition efficiency and reversibility of bacterial adhesion under flow, J. Colloid Interf. Sci., 176 (1995) 329–341.
[25] L.G. Shen, Q. Lei, J.R. Chen, H.C. Hong, Y.M. He, H.J. Lin, Membrane fouling in a submerged membrane bioreactor: Impacts of floc size, Chem. Eng. J., 269 (2015) 328–334.
[26] M. Zhang, B.Q. Liao, X. Zhou, Y. He, H. Hong, H. Lin, J. Chen, Effects of hydrophilicity/hydrophobicity of membrane on membrane fouling in a submerged membrane bioreactor, Bioresour. Technol., 175 (2015) 59–67.
[27] P. Sharma, K.H. Rao, Analysis of different approaches for evaluation of surface energy of microbial cells by contact angle goniometry, Adv. Colloid Interface Sci., 98 (2002) 341–463.
[28] Y. Zhao, F. Li, M.T. Carvajal, M.T. Harris, Interactions between bovine serum albumin and alginate: an evaluation of alginate as protein carrier, J. Colloid Interface Sci., 332 (2009) 345–353.
[29] B. Bjellqvist, G.J. Hughes, C. Pasquali, N. Paquet, F. Ravier, J.C. Sanchez, S. Frutiger, D. Hochstrasser, The focusing positions of polypeptides in immobilized pH gradients can be predicted from their amino acid sequences, Electrophoresis, 14 (1993) 1023–1031.
[30] J.P. Fuenzalida, P.K. Nareddy, I. Moreno-Villoslada, B.M. Moerschbacher, M.J. Swamy, S. Pan, M. Ostermeier, F.M. Goycoolea, On the role of alginate structure in complexing with lysozyme and application for enzyme delivery, Food Hydrocolloid., 53 (2016) 239–248.
[31] C.W. Carr, Studies on the binding of small ions in protein solutions with the use of membrane electrodes. II. The binding of calcium ions in solutions of bovine serum albumin, Arch. Biochem. Biophys., 43 (1953) 147–156.
[32] S. Damodaran, Functional properties, Food proteins: Properties and characterization, 1996, pp. 167–234.
[33] R. Kuroki, Y. Taniyama, C. Seko, H. Nakamura, M. Kikuchi, M. Ikehara, Design and creation of a Ca^{2+} binding site in human lysozyme to enhance structural stability, Proc. Natl. Acad. Sci., 86 (1989) 6903–6907.
[34] K. Nitta, H. Tsuge, S. Sugai, K. Shimazaki, The calcium-binding property of equine lysozyme, FEBS Lett., 223 (1987) 405–408.
[35] W.J. Leo, A.J. McLoughlin, D.M. Malone, Effects of sterilization treatments on some properties of alginate solutions and gels, Biotechnol. Progr., 6 (1990) 51–53.
[36] K. Katsoufidou, S. Yiantsios, A. Karabelas, Experimental study of ultrafiltration membrane fouling by sodium alginate and flux recovery by backwashing, J. Membr. Sci., 300 (2007) 137–146.
[37] H. Zheng, Q. Zhang, K. Jiang, H. Zhang, J. Wang, Critical behavior of viscosity for alginate solutions near the gelation threshold induced by cupric ions, J. Chem. Phys., 105 (1996) 7746–7752.
[38] G.T. Grant, E.R. Morris, D.A. Rees, P.J. Smith, D. Thom, Biological interactions between polysaccharides and divalent cations: the egg-box model, FEBS Lett., 32 (1973) 195–198.
[39] G. Naidu, S. Jeong, S.-J. Kim, I.S. Kim, S. Vigneswaran, Organic fouling behavior in direct contact membrane distillation, Desalination, 347 (2014) 230–239.
[40] S. Lee, W.S. Ang, M. Elimelech, Fouling of reverse osmosis membranes by hydrophilic organic matter: implications for water reuse, Desalination, 187 (2006) 313–321.
[41] Y. Ding, Y. Tian, Z. Li, H. Wang, L. Chen, Interaction energy evaluation of the role of solution chemistry and organic foulant composition on polysaccharide fouling of microfiltration membrane bioreactors, Chem. Eng. Sci., 104 (2013) 1028–1035.
[42] L. Chen, Y. Tian, C.-q. Cao, J. Zhang, Z.-n. Li, Interaction energy evaluation of soluble microbial products (SMP) on different membrane surfaces: role of the reconstructed membrane topology, Water Res., 46 (2012) 2693–2704.
[43] C. Liu, L. Chen, L. Zhu, Fouling behavior of lysozyme on different membrane surfaces during the MD operation: An especial interest in the interaction energy evaluation, Water Res., 119 (2017) 33–46.
[44] J.A. Redman, S.L. Walker, M. Elimelech, Bacterial adhesion and transport in porous media: Role of the secondary energy minimum, Environ. Sci. Technol., 38 (2004) 1777–1785.
[45] E.M. Hoek, S. Bhattacharjee, M. Elimelech, Effect of membrane surface roughness on colloid-membrane DLVO interactions, Langmuir, 19 (2003) 4836–4847.
[46] Y. Ding, Y. Tian, Z. Li, H. Wang, L. Chen, Microfiltration (MF) membrane fouling potential evaluation of protein with different ion strengths and divalent cations based on extended DLVO theory, Desalination, 331 (2013) 62–68.
[47] E.R. Morris, A.N. Cutler, S.B. Ross-Murphy, D.A. Rees, J. Price, Concentration and shear rate dependence of viscosity in random coil polysaccharide solutions, Carbohydr. Polym., 1 (1981) 5–21.

Supplementary Captions

In our previous study, peak shift and changes of peak shape were observed in the FTIR spectra of organics with and without heating, which suggest conformational changes due to the heat treatment.

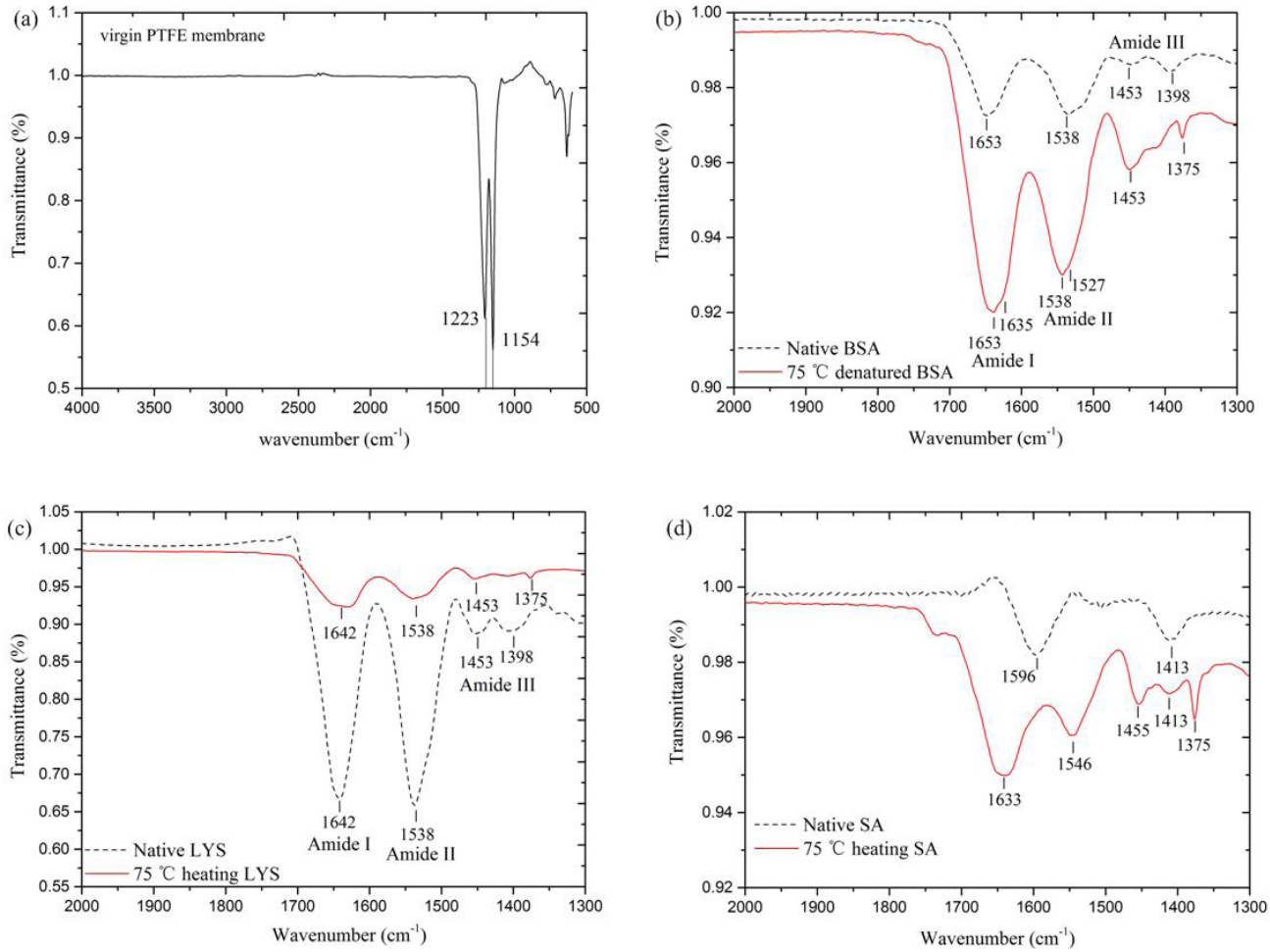

Fig. S1. FTIR spectra of the virgin membrane as well as the fouled membranes by individual organic (native form and heated form). (a) virgin PTFE membrane; (b) individual BSA; (c) individual LYS; (d) individual SA;

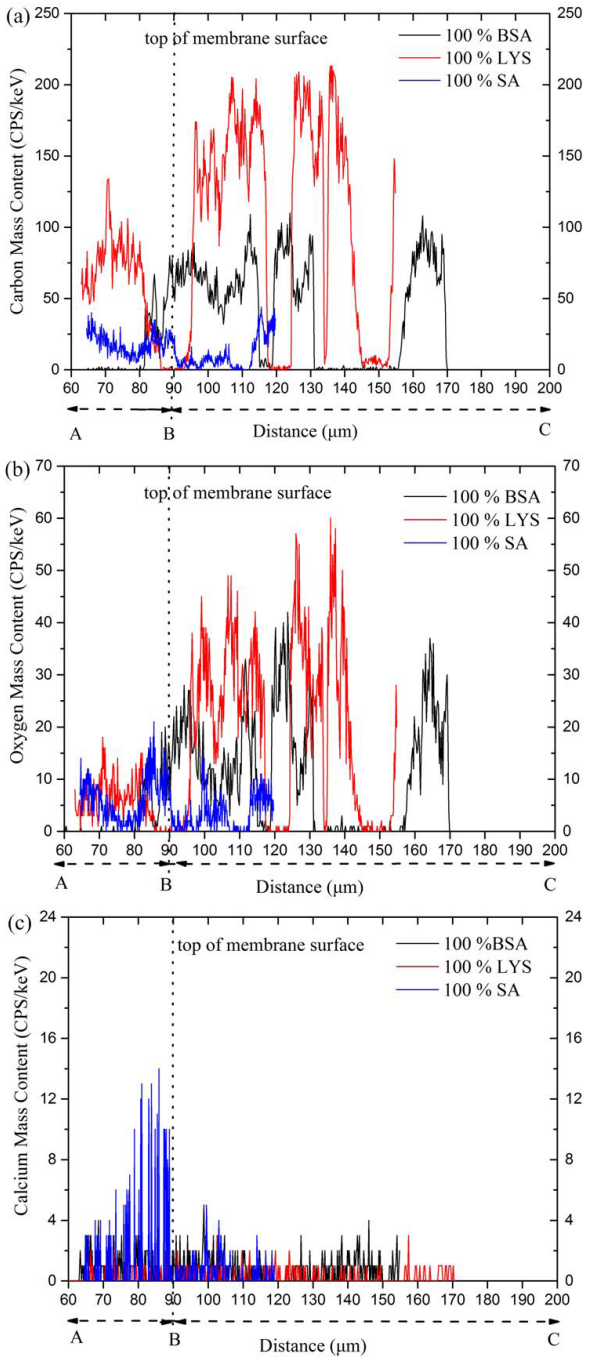

Fig. S2. EDX membrane cross section line analysis. (a) carbon element mass as a function of membrane depth; (b) oxygen element mass as a function of membrane depth; (c) calcium element mass as a function of membrane depth.

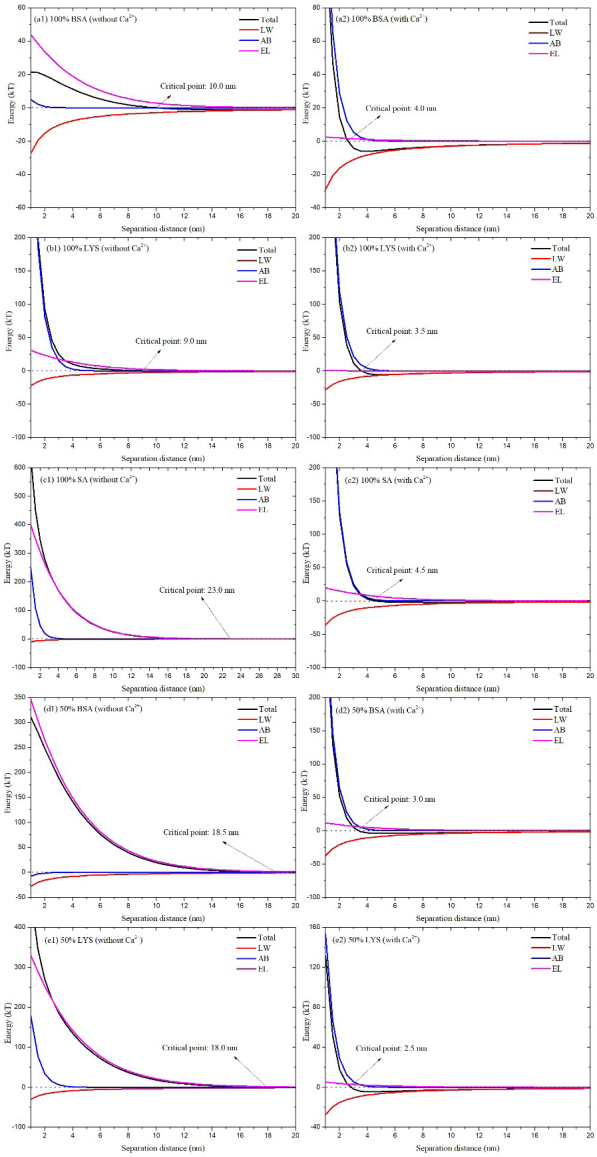

Fig. S3. Interaction energies profiles between different foulants as a function of separation distance: (a) 100% BSA; (b) 100% %LYS; (c) 100% SA; (d) 50% BSA+50% SA; (e) 50% LYS+50% SA.